2014 IEEE/RSJ International Conference on
Intelligent Robots and Systems (IROS 2014)
September 14-18, 2014, Chicago, IL, USA

Online Identification of Abdominal Tissues *In Vivo* for Tissue-Aware and Injury-Avoiding Surgical Robots

Astrini Sie, Michael Winek, and Timothy M. Kowalewski, PhD

Abstract— **This work presents a "smart" robotic surgical grasper capable of identifying tissue during the early stages of a grasp, allowing automated prevention of grasper-induced tissue crush injuries. It employs no additional sensors beyond signals already present in surgical robots. An estimation algorithm using an extended Kalman filter (EKF) is employed for a nonlinear tissue dynamic model, which is investigated *in silico* as well as *in vivo* and *in situ* on porcine models. Results show that while the approach is sensitive to initial conditions, tissue can be identified during the early stage of a typical grasp.**

I. Introduction

Migration of surgical procedures in the abdominal cavity from open surgery to minimally invasive (laparoscopic) surgery has created advantages such as reduced blood loss, improved cosmesis, faster recovery time, and shorter hospitalization period [1]–[3]. At the same time, devices used for performing laparoscopic surgery are not equipped with any force or position sensors, while in robotic surgery the graspers are equipped with only position control with no information on force. This leads to a loss of sense of touch (tactile feedback) and force (haptic feedback) from the tissue. Such absences may result in the inability to "feel" different tissue types and conditions, and in the unintentional application of excessive forces on tissue that leads to increase in chances of tissue-related injuries such as ileus, scar formation, bleeding, adhesions, perforation, hemorrhage, and tissue ischemia [4]–[8]. However, even if haptics were implemented despite its prohibitive cost, surgeons may still incorrectly interpret or ignore this information and err in judging tissue type or condition, inadvertently causing crush injury.

Prior art developed "atraumatic" graspers by mechanical [9], [10] and instrumented means [11]–[15]. While mechanical "atraumatic" graspers claim to reduce grasping pressure, the instrumented graspers are equipped with sensors that measure various tissue properties and have fused such data to provide surgeons information on force exerted at the handle or to help detect tissue ischemia. However, they did not address the variety of grasping scenarios for various tissues, and the fact that different tissues have unique optimal forces and maximum force thresholds. Although it is possible to limit maximum force exerted to tissue based on the lowest tissue-specific stress threshold available or under investigation in [16], this amount of force is not necessarily adequate to handle tougher or more massive tissue types.

These gaps motivate an instrumented grasper capable of differentiating tissues online. This can enable dedicated control algorithms tailored for the specific tissue identified. Such a tool need not provide tactile and haptic feedback but will be able to mitigate grasper-induced injuries due to excessive application of force. We herein propose to identify tissue during the early part of a grasp by a robotic surgical tool to enable tissue-specific control laws that can, for example, throttle force to avoid tissue-specific injuries. We focus on the position and force signals *already present* in typical surgical robots, and avoid requiring additional sensors at the tool tip. Thus, if our algorithm is implemented, a surgical robot may be able to guarantee atraumatic grasping.

In order to perform tissue differentiation, information on tissue properties has to be available. Models of soft tissue under force application include viscoelastic [17], polynomial [18], and Hunt-Crossley [19] models. Most existing work assumes linear tissue models to reduce complexity such as the mass-spring-damper [20] and Kelvin-Voigt models [21]. In [22], Rosen et al. performed extensive characterization of tissue biomechanical properties of *in vivo* porcine abdominal tissues, where eight tissue elastic models were proposed and the corresponding tissue properties describing each of the equations were estimated based on nonlinear regression on experimental data. Most presented tissue models only involve properties that describe tissue steady-state behavior. However, during surgery, tissue may never reach steady state conditions or it stays in steady state for a very brief period and then transitions into another steady state due to typical fast "grasp and release" motions. In [23], Yu et al. proposed incorporating linear dynamics into a Rosen's verified nonlinear mass-spring-damper tissue model [22] which allowed for characterization of tissue behavior during both the transient state and steady state. Parameter estimation of elastic tissue models have been performed using extended Kalman filters [24], recursive least squares, adaptive identification, and multi-estimator algorithms [25]. These algorithms were implemented to estimate stiffness coefficients of various silicone-based materials that act as artificial tissues. No prior work has explored or verified tissue parameter estimation *in vivo* or *in situ* in animals using robotic tools.

In this work, we present an algorithm to identify tissue types during grasping *in vivo* and *in situ* of porcine abdominal tissues using signals already available in existing surgical robots.

II. Methods

A. Pre-experimental Hardware Design

In this work, we build on a robotic grasper based on the Mechanical Smart Endoscopic Grasper (MSEG) developed in

All authors are with the Department of Mechanical Engineering at the University of Minnesota, Minneapolis, MN 55455, USA. For correspondence, contact Astrini Sie at astrini@umn.edu

[15] and the Motorized Endoscopic Grasper (MEG) developed in [13], and adapt the name *Smart Tool*. The Smart Tool is capable of quantifying force and deformation of tissue. The grasper is equipped with sensors and actuators at the handle (proximal end). The force and deformation at the grasper jaws (distal end) are obtained by transfer functions we derived using static and geometric analysis.

B. Identification of Tissue Grasping Simulations and In Vivo and In Situ on Porcine Tissues

The extended Kalman filter (EKF) algorithm is selected for online identification of four tissue types: liver (LV), small bowel (SB), bladder (BL), and gallbladder (GL); and initially verified by applying it on data of tissue grasping simulations. The first scheme is *verification* whereby a close initial guess is given to the EKF. The second scheme is *blind identification* whereby for a set of data, four parallel EKFs corresponding to four different initial tissue guesses are each applied to the data. Tissue is identified by comparing parameters and variables from the four different EKF estimation results. Next, the EKF algorithm is used to analyze data obtained from grasping experiments of *in vivo* and *in situ* porcine abdominal tissues using the robotic laparoscopic grasper.

III. The *Smart Tool*

A. Kinematic Mechanism, Sensors, and Actuators

The kinematic mechanism of the Smart Tool is that of the MSEG. The driving actuator is a brushed DC motor (RE25, Maxon Motor, Switzerland) that is connected to a capstan through a 19:1 planetary gearbox (GP26, Maxon Motor, Switzerland). The capstan is connected to a partial pulley via a 0.024 inch uncoated stainless steel cable (#2024, Sava Industries, NJ, USA). Rotating motion of the partial pulley drives the Babcock grasper head (#33510 BL, Karl Storz, Germany) through an internal scissor linkage mechanism.

The Smart Tool includes a pair of parallel strain gages (FBB300, 40lb, FUTEK, CA, USA) attached to the partial pulley that measures force exerted at the handle (proximal end). Also, there is a 500 count-per-revolution (CPR) rotary differential encoder (HEDL-5540#A02, Avago, CA, USA) connected to the motor shaft that derives tissue displacement (grasper jaws displacement) from the motor angular displacement. In addition to the existing sensors from the MSEG, in the Smart Tool, at the grasper jaws, we added two pieces of insulated wire wrapped in between the teeth. Each wire is connected to a touch sensor (1129_1, Phidgets, Alberta, Canada) to detect the time instant when the grasper jaws are in contact with tissue. This helps detect the initial tissue thickness and actual tissue displacement as opposed to total jaw displacement, but was only used to verify our system's contact identification and not for our *in vivo* and *in situ* analysis. Location of the strain gages and encoder are shown along with the configuration of the touch sensors in Fig. 1.

Sterilization is not an issue for the Smart Tool as all the additional electronics are added at the proximal end hence will not be in contact with tissue.

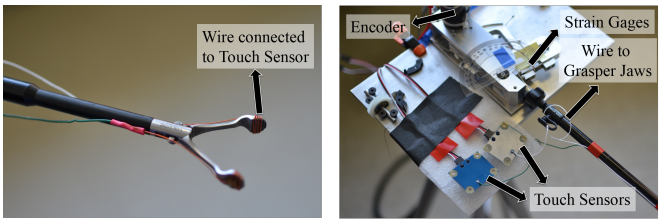

Fig. 1. The *Smart Tool*: (Left) Jaw; (Right) Handle with touch sensors configuration

B. Software-Hardware Interface and Graphical User Interface (GUI)

We developed a custom software-hardware interface and GUI for the Smart Tool which is interfaced to a Windows operating system computer using the PCI6230 module (National Instruments, TX, USA). The GUI for the Smart Tool is developed in LabVIEW (National Instruments, TX, USA). The motor current command is a trapezoidal waveform to mimic a typical grasping and releasing motion. All signals are sampled and logged at the rate of 1kHz. Raw data from strain gage and encoder is filtered with a second order Butterworth filter with cutoff frequency of 10Hz. The value is selected based on our grasp trajectory and the work performed in [26], in which the range of frequencies of typical surgical signals is characterized.

C. Grasper Handle to Grasper Jaws Transfer Functions

The readings obtained from the strain gages and encoder are in the units of voltage and degree and representing parameters at the partial pulley in the handle. Transfer functions that map the force and displacement exerted at the handle to those experienced by the tissue at the grasper jaws have to be derived.

In this work, we derive the handle force and jaws force relationship using static analysis of the grasper. We assume that all components of the grasper are stiff and have negligible deformations relative to the deformations of soft tissues. This is particularly valid at our low grasping force levels. Fig. 2 shows the diagrams of grasper handle and grasper jaws. Equation (1) shows the relationship between the raw strain gage reading at the partial pulley $V_{straingage}$ (V) and the converted force value at the handle F_{handle} (N) based on [27]. Finally, (2) shows the transfer function that relates force at the handle and force at the grasper jaws F_{jaw} (N) (equivalent to force at the tissue).

$$F_{handle} = 11.89 V_{straingage} \tag{1}$$

$$\begin{aligned} F_{jaw} = \frac{L_2 R_{pp} F_{handle}}{2 L_{jaw} a} \Bigg[& \tan\left\{ \sin^{-1}\left(\frac{L_2}{L_1} \sin(\beta_0 + \theta_{jaw}) \right) \right\} \\ & \cos\left\{ \sin^{-1}\left(\frac{L_2}{L_1} \sin(\beta_0 + \theta_{jaw}) \right) \right\} \\ & + \sin(\beta_0 + \theta_{jaw}) \Bigg] \cos\theta_{jaw} \end{aligned} \tag{2}$$

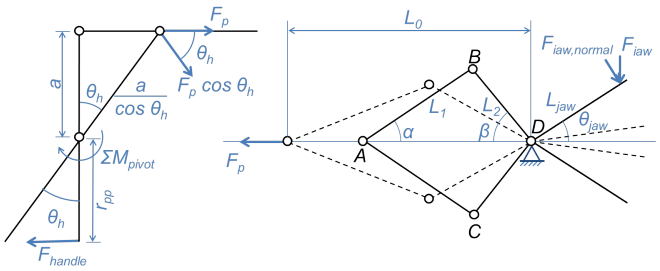

Fig. 2. Free body diagram of partial pulley (handle) and pushrod (left); grasper jaw connected to pushrod via scissor linkage mechanism (right)

We derive the displacement transfer function using geometric analysis. The angular displacement reading displayed by the encoder is dependent on force, which means a force correction factor has to be subtracted from the encoder values. Equations (3) to (5) show the correction factor $\theta_{correction}$ (°) for the raw encoder angle $\theta_{enc,raw}$ (°). The corrected encoder angle θ_{enc} (°) is then converted into the angular displacement of the partial pulley θ_{handle} (°) by the factor shown in (5). Finally, (6) shows the transfer function that relates tissue displacement to angular displacement at the handle.

$$\theta_{correction} = 52.189 V_{straingage} \tag{3}$$

$$\theta_{enc} = \theta_{enc,raw} - \theta_{correction} \tag{4}$$

$$\theta_{handle} = \frac{18}{188}\theta_{enc} \tag{5}$$

$$d = L_{jaw}\sin\left[-\beta_0 + \cos^{-1}\left(\frac{2L_2L_0\cos\beta_0 + (a\tan(\theta_{handle}))^2 - 2L_0 a\tan(\theta_{handle})}{2L_2(L_0 - a\tan(\theta_{handle}))}\right)\right] \tag{6}$$

Table I shows the values of the measured grasper geometries. The process of obtaining transfer functions from grasper handle to jaws is summarized visually in Fig. 3.

TABLE I
THE MEASURED VALUES OF ALL GRASPER LINKS LENGTHS AND OTHER RELEVANT GRASPER GEOMETRY

Grasper Geometry	Values	Grasper Geometry	Values
r_{pp}	73.15 mm	L_2	5.7 mm
a	10.1 mm	L_{jaw}	27.88 mm
L_0	9.93 mm	β_0	18.939°
L_1	4.9 mm		

IV. TISSUE IDENTIFICATION ALGORITHM DEVELOPMENT

In this work, we employ an extended Kalman filter (EKF) algorithm for identifying tissue grasped online by estimating tissue parameters based on a nonlinear tissue dynamic model. This algorithm is chosen as it is computationally fast and good for estimating *states* of a dynamic data that vary over time.

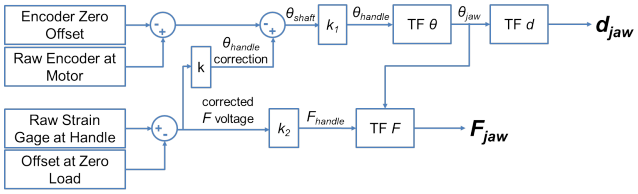

Fig. 3. Flowchart of process from raw strain gage and encoder data to force and displacement at tissue

A. Algorithm Design

A mathematical dynamic model of tissue during grasping is approximated in [23] as shown in (7). u (N) is force applied to tissue, x (m) is tissue displacement (m), m (kg) is mass of tissue grasped, d (kg s^{-1}) is tissue damping coefficient, and α (N) and β (m^{-1}) are tissue stiffness coefficients.

The system model is re-written as (8) and restated as a state-space model in the continuous-time linear form shown (9). $\mathbf{x} = \begin{bmatrix} x & \dot{x} & \alpha & \beta & d \end{bmatrix}^T$ is the state vector. α, β, and d are augmented to the state vector such that the three parameters are to be estimated with the EKF. $\mathbf{u} = \begin{bmatrix} u & 0 & 0 & 0 \end{bmatrix}^T$ is the input vector. $\mathbf{w} = \begin{bmatrix} 0 & w_\alpha & w_\beta & w_d \end{bmatrix}^T$ is the disturbance vector of process noise that enters α, β, and d. F and G are the continuous-time state and input matrices.

$$u = m\ddot{x} + d\dot{x} + \alpha(e^{\beta x} - 1) \tag{7}$$

$$\ddot{x} = f(\mathbf{x}) + g(\mathbf{u}) = -\frac{d}{m}\dot{x} - \frac{\alpha}{m}(e^{\beta x} - 1) + \frac{1}{m}u \tag{8}$$

$$\dot{\mathbf{x}} = F\mathbf{x} + G(\mathbf{u} + \mathbf{w}) \tag{9}$$

The state matrix F is obtained by taking the Jacobian of the state equation (8). The input matrix G is shown in (11). The hat notation ($\hat{\mathbf{x}}$) denotes estimated variables. The process covariance matrix P is shown in (12), and the process noise covariance matrix Q_w is shown in (13). Both covariance matrices are chosen to be diagonal. x and $\dot{x}$ are uncorrelated in the process, and we assume that α, β, and d are uncorrelated among each other as well. In the process noise, all the four parameters are assumed uncorrelated.

$$F = \begin{bmatrix} 0 & 1 & 0 & 0 & 0 \\ -\frac{1}{m}\hat{\alpha}\hat{\beta}e^{\hat{\beta}\hat{x}} & -\frac{1}{m}\hat{d} & -\frac{1}{m}\hat{\beta}\hat{x} + \frac{1}{m} & -\frac{1}{m}\hat{\alpha}\hat{x}e^{\hat{\beta}\hat{x}} & -\frac{1}{m}\hat{x} \\ 0 & 0 & 0 & 0 & 0 \\ 0 & 0 & 0 & 0 & 0 \\ 0 & 0 & 0 & 0 & 0 \\ 0 & 0 & 0 & 0 & 0 \end{bmatrix} \tag{10}$$

$$G = \begin{bmatrix} 0 & 0 & 0 & 0 \\ \frac{1}{m} & 0 & 0 & 0 \\ 0 & 1 & 0 & 0 \\ 0 & 0 & 1 & 0 \\ 0 & 0 & 0 & 1 \end{bmatrix} \tag{11}$$

$$P = diag(\sigma_x^2, \sigma_{\dot{x}}^2, \sigma_\alpha^2, \sigma_\beta^2, \sigma_d^2) \tag{12}$$

$$Qw = diag(\sigma_{w,u}^2, \sigma_{w,\alpha}^2, \sigma_{w,\beta}^2, \sigma_{w,d}^2) \tag{13}$$

The continuous-time matrices are converted into their discrete-time equivalents as shown in (14) and (15). dt is the sampling interval that is equal to the sampling rate (1ms).

$$\Phi = e^{Fdt} \tag{14}$$

$$Q = GQ_wG^T dt \tag{15}$$

The measurement model for the EKF comes from the sensors attached to the system, which measure: tissue displacement x (encoder), and force applied by the motor at the handle u (strain gages). The measurement equation is shown in (16). $\mathbf{y}$ is the output vector which consists of only the displacement x. H is the continuous-time output matrix, as shown in (17). Noise in the measurement is considered in this work by having measurement covariance matrix R as depicted in (18).

$$\mathbf{y} = H\mathbf{x} + \mathbf{v} \tag{16}$$

$$H = \begin{bmatrix} 1 & 0 & 0 & 0 & 0 \end{bmatrix} \tag{17}$$

$$R = \sigma_{r,x}^2 \tag{18}$$

In the first stage of the EKF (the time update or prediction), the state variables to be estimated are propagated in time from the estimates at the previous time step. The time updates for the state variables are shown in (19). The $-$ notation indicates state variable prior to time update, and the $+$ notation indicates state variable after the time update. During the time update, the process covariance matrix P is also updated in time as shown in (20).

$$\begin{aligned}
\hat{x}(t)^- &= \hat{x}(t-1)^+ + \hat{\dot{x}}(t-1)^+ dt \\
\hat{\dot{x}}(t)^- &= \hat{\dot{x}}(t-1)^+ + \hat{\ddot{x}}(t-1)dt \\
\hat{\ddot{x}}(t-1) &= -\frac{\hat{d}(t-1)\hat{\dot{x}}(t-1)}{m} - \frac{\hat{\alpha}(t-1)}{m}\left(e^{\hat{\beta}(t-1)\hat{x}(t-1)} - 1\right) \\
&\quad + \frac{u(t-1)}{m} \\
\hat{\alpha}(t)^- &= \hat{\alpha}(t-1)^+ \\
\hat{\beta}(t)^- &= \hat{\beta}(t-1)^+ \\
\hat{d}(t)^- &= \hat{d}(t-1)^+
\end{aligned} \tag{19}$$

$$P(t)^- = \Phi P(t-1)^+ \Phi^T + Q \tag{20}$$

After the time update, the state variables are corrected according to the typical discrete EKF.

B. Simulation of Tissue Model during Grasping

A tissue nonlinear model based on (7) is created in *SIMULINK*. All parameters used for the simulation are shown in Table II, where m is tissue mass, A_{jaw} is the surface area of grasper jaw, x_0 is initial tissue thickness, α and β are tissue stiffness coefficients, d is tissue damping coefficient, and p_{thres} is the anticipated pressure threshold of tissue at which damage may occur based on [4]. α and β values for different tissues are adapted from values obtained by Brown et al. in [28] for soft tissue models as basic exponential functions ($\sigma = \bar{\alpha}(e^{\bar{\beta}\varepsilon} - 1)$). We adapt the following notation:

TABLE II
PARAMETERS USED FOR SIMULATION OF NONLINEAR MODEL OF SOFT TISSUE DURING GRASPING

Parameters	Tissue Types			
	Liver (LV)	Small Bladder (SB)	Bladder (BL)	Gallbladder (GB)
m (kg)	0.005			
A_{jaw} (mm^2)	56.3			
x_0 (mm)	7.5	5.5	26	26
$\bar{\alpha}$ (N)	849.2	518.9	0.005	379.3
$\bar{\beta}$ (m^{-1})	14.32	11.87	20.46	11.26
d (kg s^{-1})	3.1	3.3	1.3	0.5
p_{thres} (kPa)	60	100	40	40

$$\begin{aligned}
&\text{Stress-strain relationship in [28]:} \quad \sigma = \bar{\alpha}(e^{\bar{\beta}\varepsilon} - 1) \\
&\text{Force-displacement relationship:} \quad F = \alpha(e^{\beta x} - 1) \\
&\sigma = \frac{F}{A_{jaw}} \quad \varepsilon = \frac{x - x_0}{x_0} \\
&\alpha = \bar{\alpha}(A_{jaw}) \quad \beta = \frac{\bar{\beta}}{x_0}
\end{aligned} \tag{21}$$

Inputs of sinusoidal force with magnitude of 2N and frequency of 4Hz are used. The maximum input force of 2N is chosen as it was the smallest maximum tolerable force among the abdominal tissues before any injuries [4]. Input frequency of 4Hz is chosen to represent fastest typical grasping rate used by clinicians. The first sinusoidal wave is set to be at 2Hz to allow for tissue detection to be completed before a full grasp in a typical simulation. The output of the simulation are the force and position data, which are used as the u and x for the EKF analysis respectively.

V. EKF IDENTIFICATION OF TISSUE GRASPING SIMULATIONS

A. Simulation Verification Results

Our EKF algorithm is implemented on tissue force u and displacement x data obtained in simulation to identify tissue types by estimating tissue stiffness (α, β) and damping (d) coefficients. The estimated states values over time (α, β, d, x) for all the four tissues are compared to the expected state values. Fig 4 (left) shows the estimated and expected states for liver tissue. In addition, Table III shows the mean of the final estimated states values from ten EKF estimation simulations performed in *MATLAB*.

Fig. 4 (right) shows the sample plot for liver tissue of the force equation $F = \alpha(e^{\beta x} - 1)$ using α and β from [28] (expected values), the force equation using estimated values of $\hat{\alpha}$ and $\hat{\beta}$, the force input to *SIMULINK* u, and the threshold force for the specific tissue type. Also, concatenated below the forces plots, force errors (estimated force subtracted with force input to *SIMULINK*) are shown. The force error threshold is chosen as 15% of the maximum input force value u.

TABLE III

STEADY STATE VALUES OF ESTIMATED STATES AND EXPECTED STATES IN EKF VERIFICATION SIMULATION

Tissue Type	Estimated States			Expected States		
	$\bar{\hat{\alpha}}$	$\bar{\hat{\beta}}$	$\bar{\hat{d}}$	$\bar{\alpha}$	$\bar{\beta}$	$\bar{d}$
LV	799.9094	14.5509	4.7069	849.2	14.32	3.1
SB	489.3628	12.0474	5.014	518.9	11.87	3.3
BL	0.0046	20.5933	2.489	0.005	20.46	1.3
GB	356.6571	11.4143	1.3985	379.3	11.26	0.5

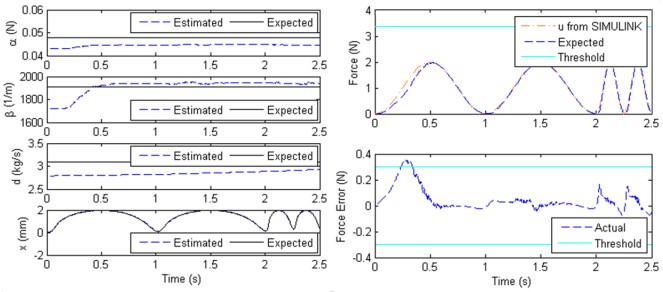

Fig. 4. (Left) Estimated states plotted together with the expected states; (Right) Plot of estimated, input, and threshold forces for simulation of liver tissue during grasping

Fig. 5 shows the stress-strain curves for all tissue types plotted using the estimated and expected values of tissue stiffness parameters.

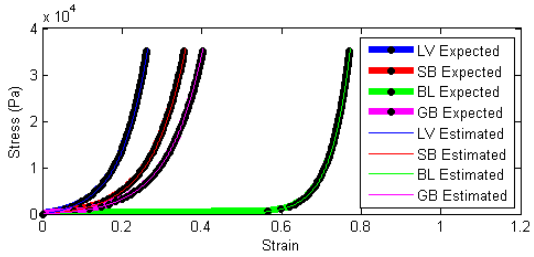

Fig. 5. Stress-strain plots for various tissue types using $\hat{\alpha}$ and $\hat{\beta}$ estimated from EKF simulation

B. Simulation Verification Discussion

Fig. 4 (left) indicates that the estimated tissue stiffness coefficients ($\hat{\alpha}$, $\hat{\beta}$) converge to steady state values within 0.5s for all tissue types. However, the estimated damping coefficient ($\hat{d}$) do not converge to a steady state value but keep increasing slowly, this is because small errors in $\hat{\alpha}$ and $\hat{\beta}$ are reflected as larger error in $\hat{d}$. However, the values of $\hat{d}$ remain relatively constant over the course of initial grasps (first 1s) hence acceptable for typical grasping speed. The estimated displacements are closely similar to the expected displacements from simulation. The final estimated values of $\hat{\alpha}$ and $\hat{\beta}$ possess some error from the expected values. However, Fig. 5 depicts that despite of the error, the stress-strain curves obtained using the estimated parameters coincide well with the actual curves using expected parameters, and that each tissue types have distinct estimated stress-strain curves.

Fig. 4 (right) indicates that the resulting force calculated using estimated values of $\hat{\alpha}$ and $\hat{\beta}$ converges with that of expected α and β with an error of lower than 15% the maximum force after 0.379s for liver, 0.354s for small bowel, 0.282s for bladder, and 0.369s for gallbladder. The convergence time indicates that the EKF designed is able to estimate force precisely within 0.4s, which is at the early part of a grasp. The convergence time and force error are summarized in Table IV.

C. Blind Identification in Simulation

In the blind identification scheme, four EKFs with different initial tissue guesses each are run on data from one particular tissue grasping session at the same time. By looking at the resulting convergence time and force error from each of the EKF simulation results as shown in Table V, the correct tissue type can be identified. It is found that in simulation, blind identification of bladder and gallbladder can be performed, but additional information has to be analyzed in order to differentiate liver and small bowel. Identification of all tissue types can be achieved by looking at the stress-strain curves of the estimated tissue stiffness parameters.

VI. EKF IDENTIFICATION OF *IN VIVO* AND *IN SITU* PORCINE TISSUES

A. Experimental Protocol

Data collections were performed *in vivo* and *in situ* on liver, small bowel, bladder, and gallbladder tissues of two porcine models in the Visible Heart Laboratory at the University of Minnesota. Fig. 6 shows the grasps performed for all four tissue types. The grasping profile applied is a trapezoidal waveform with frequencies of 2Hz and 4Hz, and force command amplitudes of 0.8N and 1.55N, well below levels that induce crush injury. The total number of single grasps for liver is 271, small bowel is 155, bladder is 173, and gallbladder is 112, giving a total of 711 grasps for all tissue types.

B. EKF Implementation and Results

Close initial guesses were chosen as the initial conditions for the EKF. The left plot in Fig. 7 shows a sample plot of estimated states together with the expected states over time for one single grasp with 0.25Hz frequency and 2V (1.55N) motor command on liver tissue. The force error between the measured force and calculated force using estimated states are computed to find the convergence time of the filter. The convergence time is defined as the latest time instant when the force error drops below and never exceeds the error threshold. The error threshold is defined as 15% of the maximum force threshold for each tissue type as in simulation. The right plot in Fig. 7 shows the plot of measured and estimated force values, and the corresponding force error and error threshold over time for one single grasp with 0.25Hz frequency and 2V (1.55N) motor command on liver tissue. Table VI shows the maximum, mean, and minimum values of convergence time and force error for all

tissue types. (Note negative force errors are conservative, i.e. safer than positive errors.)

TABLE IV
CONVERGENCE TIME AND VALUE OF FORCE ERROR OF EKF VERIFICATION SIMULATION

		Tissue Types			
		LV	SB	BL	GB
Conv. Time (s)	Max	0.425	0.380	0.292	0.425
	Mean	0.379	0.354	0.282	0.369
	Min	0.346	0.290	0.270	0.334
Force Error (N)	Max	0.405	0.398	0.610	0.413
	Mean	0.014	0.010	0.010	0.013
	Min	-0.167	-0.179	-0.300	-0.242

TABLE V
CONVERGENCE TIME AND VALUE OF FORCE ERROR OF EKF BLIND IDENTIFICATION SIMULATION

Initial Tissue Guess		Tissue Grasped			
		LV	SB	BL	GB
LV	Conv. Time (s)	0.366	0.384	1.217	6.807
	Force Error (N)	0.012	-0.008	-0.121	-0.045
SB	Conv. Time (s)	0.339	0.359	1.047	4.621
	Force Error (N)	0.034	0.011	-0.113	-0.032
BL	Conv. Time (s)	8.220	8.220	0.274	2.470
	Force Error (N)	∞	∞	0.008	∞
GB	Conv. Time (s)	9.061	9.032	1.429	0.371
	Force Error (N)	1	1	-0.134	0.013

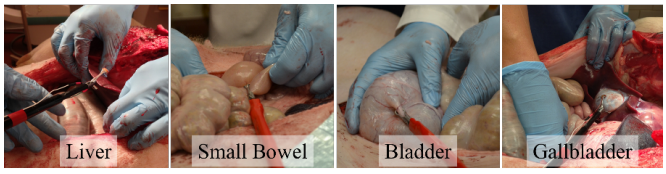

Fig. 6. Grasping sessions performed on all four tissue types

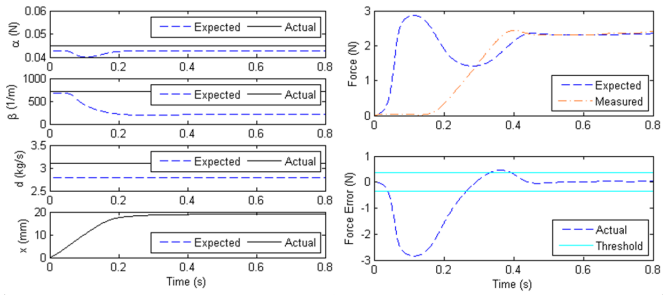

Fig. 7. (Left) Estimated and expected states; (Right) Estimated and expected force, force error and error threshold for 0.25Hz, 2V (1.55N) single grasp on liver tissue

The final or steady state estimated values of $\hat{\bar{\alpha}}$, $\hat{\bar{\beta}}$, and $\hat{\bar{d}}$ for each single grasp are plotted in the form of box plots as shown in Fig. 8. The mean of steady state $\hat{\bar{\alpha}}$, $\hat{\bar{\beta}}$, and $\hat{\bar{d}}$ for each type of tissue is shown in Table VII.

TABLE VI
CONVERGENCE TIME AND FORCE ERROR FOR PORCINE TISSUES IDENTIFICATION

		LV	SB	BL	GB
Conv. Time (s)	Max	0.727	0.768	2.419	0.714
	Mean	0.257	0.292	0.309	0.253
	Min	0.029	0.029	0.033	0.073
Force Error (N)	Max	0.679	0.470	0.965	0.668
	Mean	-0.273	-0.276	0.175	-0.177
	Min	-5.304	-1.953	-0.922	-9.325

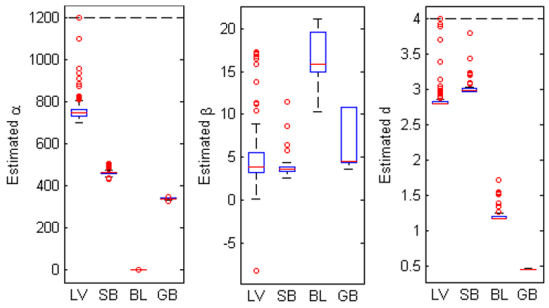

Fig. 8. Box plots of estimated $\hat{\alpha}$, $\hat{\beta}$, and $\hat{d}$ for all grasps on all four tissue types (approximately 11 extreme outliers are not shown)

TABLE VII
STEADY STATE VALUES OF ESTIMATED STATES AND EXPECTED STATES FOR PORCINE TISSUES IDENTIFICATION

Tissue Type	Estimated States (Mean)		
	$\bar{\alpha}$	$\bar{\beta}$	$\bar{d}$
LV	757.808	5.758	2.841
SB	459.157	4.321	3.004
BL	0.004	16.956	1.213
GB	336.186	6.411	0.455

C. Discussion

The significance of knowing the force error values over time or the convergence time is to ensure tissue safety, that is, before applying a force that exceeds the maximum value the tissue can tolerate, the force estimation from EKF has converged and we are able to correct the force amount delivered to the tissue by applying a control law. We can see from Table VI that the force error drops below 15% of the maximum force threshold for each tissue below 0.3s. Thus, if the early part of the grasps is performed before 0.3s, force estimation is able to be performed with acceptable accuracy before the grasp is completed.

While the force error indicates the boundary for keeping a tissue safe, the estimated states ($\hat{\bar{\alpha}}$, $\hat{\bar{\beta}}$, and $\hat{\bar{d}}$) are important for discriminating specific tissue types. This is essential before a force control algorithm throttles the force delivered to a specific tissue. Fig. 8 shows that the estimated values of $\hat{\bar{\alpha}}$ and $\hat{\bar{d}}$ for all four tissue types are distinct. Distinct estimated values of $\hat{\bar{\beta}}$ is observed for bladder and gallbladder, but overlaps is seen between liver and small bowel.

We employ Tukey's honestly significant difference criterion ($p < 0.05$) for multicomparison tests of the estimated values of $\hat{\tilde{\alpha}}$, $\hat{\tilde{\beta}}$, and $\hat{d}$ for all tissue types. Using the estimated values of $\hat{\tilde{\alpha}}$, we are able to differentiate the four tissue types. The resulting estimated values of $\hat{\tilde{\beta}}$ are unique for small bowel, bladder, and either liver or gallbladder. Using $\hat{\tilde{\beta}}$ information only, the EKF algorithm is not able to differentiate liver from small bowel. The multicomparison test for estimated $\hat{d}$ is unique for all tissue types. Thus, by using the combination of estimated results of $\hat{\tilde{\alpha}}$, $\hat{\tilde{\beta}}$, or $\hat{d}$, the EKF algorithm is able to perform unique tissue identification on *in vivo* and *in situ* porcine tissues in our data.

VII. CONCLUSIONS

In this work, we successfully developed a smart laparoscopic grasper to quantify force delivered to the tissue by grasper handle to jaws transfer functions. We designed an EKF algorithm to perform tissue identification. The EKF algorithm shows favorable force estimation times in both simulation (within 400ms) and *in vivo* (within 300ms on average). In addition to observing distinct estimated stress-strain curves, tissue identification in simulation can be performed by looking at the speed of convergence and absolute force error. These preliminary results are promising. Nevertheless, though fast, the EKF algorithm is not an ideal method due to its sensitivity to initial conditions. Future work will include applying an alternative online estimation method such as unscented Kalman filter or particle filter, transferring this work to existing surgical robotic tools, implementing force and displacement sensors directly at the grasper jaws, and also developing and evaluating control algorithms that regulate the amount of force delivered to the tissue based on the specific tissue type.

ACKNOWLEDGMENT

The authors are indebted to Dr. Blake Hannaford from the University of Washington for lending us his MSEG platform for this study. The authors would also like to thank Dr. Paul A. Iaizzo and Tinen Iles from the Visible Heart Laboratory at the University of Minnesota for the tremendous help and time provided during the data collection on porcine models.

REFERENCES

[1] J. L. Flowers, R. W. Bailey, W. A. Scovill, and K. A. Zucker, "The Baltimore Experience with Laparoscopic Management of Acute Cholecystitis," *Am. J. Surg.*, vol. 161, no. 3, pp. 388–392, 1991.

[2] K. A. Zucker, R. W. Bailey, T. R. Gadacz, and A. L. Imbembo, "Laparoscopic Guided Cholecystectomy," *Am. J. Surg.*, vol. 161, no. 1, pp. 36–44, 1991.

[3] A. Cuschieri, J. Hunter, B. Wolfe, L. Swanstrom, and W. Hutson, "Multicenter Prospective Evaluation of Laparoscopic Antireflux Surgery," *Surg. Endosc.*, vol. 7, no. 6, pp. 505–510, 1993.

[4] S. De, "The Grasper-Tissue Interface in Minimally Invasive Surgery: Stress and Acute Indicators of Injury," Ph.D. dissertation, Department of Bioengineering, University of Washington, June 2008.

[5] J. Kalff, T. Carlos, W. Schraut, T. Billiar, R. Simmons, and A. Bauer, "Surgically Induced Leukocytic Infiltrates within the Rat Intestinal Muscularis Mediate Postoperative Ileus," *Gastroenterology*, vol. 117, no. 2, pp. 378–387, 1999.

[6] R. Anup and K. Balasubramanian, "Surgical Stress and the Gastrointestinal Tract," *J. Surg. Res.*, vol. 92, no. 2, pp. 291–300, 2000.

[7] E. Heijnsdijk, J. Dankelman, and D. Gouma, "Effectiveness of Grasping and Duration of Clamping Using Laparoscopic Graspers," *Surg. Endosc.*, vol. 16, no. 9, pp. 1329–1331, 2002.

[8] D. Marucci, A. Shakeshaft, J. Cartmill, M. Cox, S. Adams, and C. Martin, "Grasper Trauma During Laparoscopic Cholecystectomy," *Aust. N. Z. J. Surg.*, vol. 70, no. 8, pp. 578–581, 2000.

[9] D. Sugarbaker, A. Levine, N. Warner, E. May, and L. Crainich, "Tissue Grasping Device," U.S. Patent 5,928,264, July 27, 1999.

[10] R. D. Adams and S. E. Thompson, "Atraumatic Endoscopic Apparatus," European Patent Patent EP0 598 607, February 16, 2000.

[11] B. Ristic, S. Kun, and R. Peura, "Development of an Impedance Spectrometer for Tissue Ischemia Monitoring: Application of Synchronous Sampling Principle," in *IEEE 21st Annu. Northeast Bioengineering Conf.* IEEE, 1995, pp. 74–75.

[12] J. Rosen, B. Hannaford, M. MacFarlane, and M. Sinanan, "Force Controlled and Teleoperated Endoscopic Grasper for Minimally Invasive Surgery - Experimental Performance Evaluation," *IEEE Trans. Biomed. Eng.*, vol. 46, no. 10, pp. 1212–1221, 1999.

[13] J. Brown, J. Rosen, M. Moreyra, M. Sinanan, and B. Hannaford, "Computer-controlled Motorized Endoscopic Grasper for In Vivo Measurement of Soft Tissue Biomechanical Characteristics," *Stud. Health Technol. Inform.*, pp. 71–73, 2002.

[14] G. Fischer, T. Akinbiyi, S. Saha, J. Zand, M. Talamini, M. Marohn, and R. Taylor, "Ischemia and Force Sensing Surgical Instruments for Augmenting Available Surgeon Information," in *IEEE RAS & EMBS Int. Conf. Biomed. Robot. Biomechatronics*. IEEE, 2006, pp. 1030–1035.

[15] P. R. Roan, "An Instrumented Surgical Tool for Local Ischemia Detection," Ph.D. dissertation, Department of Electrical Engineering, University of Washington, 2011, copyright ProQuest, UMI Dissertations Publishing 2011. [Online]. Available: http://search.proquest.com/docview/888466235?accountid=14784

[16] S. De, J. Rosen, A. Dagan, B. Hannaford, P. Swanson, and M. Sinanan, "Assessment of Tissue Damage due to Mechanical Stresses," *Int. J. Rob. Res.*, vol. 26, no. 11-12, pp. 1159–1171, 2007.

[17] H. W. Haslach Jr, "Nonlinear Viscoelastic, Thermodynamically Consistent, Models for Biological Soft Tissue," *Biomech. Model. Mechanobiol.*, vol. 3, no. 3, pp. 172–189, 2005.

[18] A. Bicchi, G. Canepa, D. De Rossi, P. Iacconi, and E. Scillingo, "A Sensor-Based Minimally Invasive Surgery Tool for Detecting Tissue Elastic Properties," in *IEEE Int. Conf. Robot. Automat.*, vol. 1. IEEE, 1996, pp. 884–888.

[19] K. Hunt and F. Crossley, "Coefficient of Restitution Interpreted as Damping in Vibroimpact," *J. Appl. Mech.*, 1975.

[20] E. Turgay, S. Salcudean, and R. Rohling, "Identifying the Mechanical Properties of Tissue by Ultrasound Strain Imaging," *Ultrasound Med. Biol.*, vol. 32, no. 2, pp. 221–235, 2006.

[21] L. S. Taylor, A. L. Lerner, D. J. Rubens, and K. J. Parker, "A Kelvin-Voigt Fractional Derivative Model for Viscoelastic Characterization of Liver Tissue," in *ASME Int. Mech. Eng. Congr. and Expo.*, 2002.

[22] J. Rosen, J. D. Brown, S. De, M. Sinanan, and B. Hannaford, "Biomechanical Properties of Abdominal Organs In Vivo and Postmortem Under Compression Loads," *J. Biomech. Eng.*, vol. 130, pp. 021 020–1, 2008.

[23] X. Yu, H. J. Chizeck, and B. Hannaford, "Comparison of Transient Performance in the Control of Soft Tissue Grasping," in *IEEE/RSJ Int. Conf. Intell. Robots Syst.* IEEE, 2007, pp. 1809–1814.

[24] T. Hoshi, Y. Kobayashi, and M. Fujie, "Developing a System to Identify the Material Parameters of an Organ Model for Surgical Robot Control," in *IEEE RAS & EMBS Int. Conf. Biomed. Robot. Biomechatronics*. IEEE, 2008, pp. 730–735.

[25] T. Yamamoto, M. Bernhardt, A. Peer, M. Buss, and A. M. Okamura, "Techniques for Environment Parameter Estimation during Telemanipulation," in *IEEE RAS & EMBS Int. Conf. Biomed. Robot. Biomechatronics*. IEEE, 2008, pp. 217–223.

[26] T. M. Kowalewski, "Real-time Quantitative Assessment of Surgical Skill," Ph.D. dissertation, University of Washington, 2012.

[27] A. Sie and T. M. Kowalewski, "Quantifying Forces at the Tool-Tissue Interface of a Surgical Laparoscopic Grasper," *J. Med. Devices*, vol. 7, pp. 030 913–030 913–2, 2013.

[28] J. D. Brown, J. Rosen, Y. S. Kim, L. Chang, M. N. Sinanan, and B. Hannaford, "In-vivo and In-situ Compressive Properties of Porcine Abdominal Soft Tissues," *Stud. Health Technol. Inform.*, pp. 26–32, 2003.